

Laser-controlled field effect in graphene/hexagonal boron nitride heterostructures

I. Wlasny,^{1, a)} R. Stepniewski,¹ Z. Klusek,² W. Strupinski,^{3, 4} and A. Wyszomolek¹

¹⁾*Institute of Experimental Physics, Faculty of Physics, University of Warsaw, Pasteura 5, 02-093 Warsaw, Poland*

²⁾*Department of Solid State Physics, Faculty of Physics and Applied Informatics, University of Lodz, Pomorska 149/153, 90-236 Lodz, Poland*

³⁾*Institute of Electronic Materials Technology, Wolczynska 133, 01-919 Warsaw, Poland*

⁴⁾*Faculty of Physics, Warsaw University of Technology (WUT), Koszykowa 75, 00-662 Warsaw, Poland*

(Dated: 3 December 2024; Revised 3 December 2024)

The possibility of modification of the local properties of hexagonal boron nitride (h-BN) by laser irradiation is investigated. Investigations conducted using both Raman spectroscopy and electrostatic force microscopy were performed. Laser light induced modifications are found to cause no structural changes. However, they have impact on Raman spectra and local charge state of the material. They are also shown to be stable in time and during electrical grounding of the sample. The mechanism of photoionization of deep defects present in h-BN is proposed to explain the observed phenomenon. The discussed effect opens up new method of nanostructurization of h-BN based planar heterostructures.

CONTENTS

I. Introduction	1
II. Experimental details	2
A. Sample preparation	2
B. Atomic/Electrostatic Force Microscopy	2
C. Raman Spectroscopy and Optical Microscopy	2
III. Results and discussion	2
A. Electric field measurements	2
B. Time-resolved Raman measurements	3
C. Modification stability	6
D. Response of graphene to h-BN modification	6
IV. Conclusions	7
V. Acknowledgments	8
VI. References	8

I. INTRODUCTION

Two-dimensional Van Der Waals heterostructures, in recent years, attract growing attention of the scientific and industry communities¹⁻⁴. They owe their popularity to possibility of creating planar nanodevices, which is related to the characteristics of Van Der Waals materials as well as the possibility of tailoring electrical and optical properties^{5,6}. This shows their high potential for application in various electronic or optoelectronic devices. In

particular, one of the most thoroughly investigated heterostructures are composed of graphene and hexagonal boron nitride, finding use in e.g. tunneling diodes or transistors.

Graphene is a carbon allotrope with hexagonal structure⁷. From the point of view of its electronic structure it is a zero-bandgap semiconductor with exceptionally high charge carrier mobility^{8,9}. However, in relation to the heterostructure construction, the most important aspect of graphene is that its properties are sensitive to a broad spectrum of factors, such as growth method¹⁰, interaction with a substrate¹¹ or the environmental interactions, such as a field effect¹².

Hexagonal boron nitride (h-BN) has similar structure to that of a graphene¹³, including the lattice configuration as well as a closely matching lattice constant. It is, however, a semiconductor with a bandgap over 5 eV wide¹⁴. Being dielectric⁷ it interacts weakly with graphene layers within a heterostructure. Due to aforementioned slight lattice mismatch and possible rotation periodic superstructures with new functionalities could be formed¹⁶.

In this article we investigate the controlling the 2D materials by means of modification of the h-BN charge state using focused light beam. In our study we have investigated exfoliated from bulk crystals as well as transferred CVD-grown h-BN samples. Our Raman scattering (RS) and electrostatic force microscopy (EFM) investigations indicate the possibility of locally influencing the properties of the hexagonal boron nitride as well as prove that the laser-based experimental techniques should be used with caution when investigating two-dimensional materials. They also allowed us to pinpoint the origin of observed changes as well as study their dynamics. Our investigations of the graphene/h-BN heterostructure show that the photoionization of the deep defect centers has an

^{a)}Electronic mail: igor.wlasny@fuw.edu.pl

effect on the charge carrier concentration of the graphene due to field-effect in the interlayer interaction. This is particularly important, as the same effect occurs within heterostructures basing on other 2D materials. The discussed phenomenon opens up new method of nanostucturization of the planar heterostructures based on h-BN as well as provides a new possibilities of application of graphene/h-BN structures.

II. EXPERIMENTAL DETAILS

A. Sample preparation

The investigations presented in this article have been conducted on a series of samples, allowing us to both investigate standalone h-BN layers and the effect of laser illumination on their characteristics and graphene/h-BN heterostructures, which were used to investigate the effect of h-BN modification on graphene.

First sample, later referred to as h-BN/SiO₂, was prepared by mechanical exfoliation of commercially available h-BN single crystals¹⁷. Initial exfoliation was performed using standard dicing tape (Microworld M07). Final exfoliation and transfer onto target substrate was performed with 0.1 nm thick PDMS film. Flakes were deposited onto boron doped (p-type) substrate (resistivity of 1Ω-cm) with 90 nm of the thermal oxide. Such substrate enhances the optical contrast of the h-BN flakes allowing for their quick and easy identification¹⁸. The PDMS film was removed from SiO₂ during the cooling after previously heating the sample up to 80°C, which increased the effectiveness of the deposition¹⁹.

Sample referred to h-BN/G/SiC served as a model of the heterostructure of graphene and hexagonal boron nitride. It has been prepared using exfoliation method described previously. However, instead of SiO₂/Si substrate 4H-SiC crystal with epitaxial graphene monolayer²⁰ has been used. Graphene layer was grown using a commercial horizontal CVD hot-wall reactor using the propane gas as a precursor²⁰.

Last of the samples shown in this article - G/h-BN/SiO₂ was prepared by depositing graphene and hexagonal boron nitride onto the substrate similar to that used in h-BN/SiO₂ sample. Both graphene and h-BN were synthesized using the CVD method on high purity Cu foil substrates. They were transferred onto SiO₂ with the modified wet-transfer method²¹. Before the etching of copper 0.1 mm thick PDMS layer was deposited on the h-BN/Cu. The etching was performed in 0.1 M aqueous solution of iron(III) nitrate nonahydrate at 21°C over the time span of 20 hours. PDMS with h-BN/graphene layers was cleaned of the iron(III) nitrate contamination with ten cycles of bathing in deionized water. Subsequently, PDMS with h-BN/graphene was carefully placed on the SiO₂ substrate, where it was left pressed down for 30 minutes. PDMS layer was removed during the cooling phase after previously heating the sample to 80°C,

which results in better control and higher effectiveness of the deposition process¹⁹.

B. Atomic/Electrostatic Force Microscopy

Both atomic force microscopy (AFM) and electrostatic force microscopy (EFM) measurements were performed using NT-MDT Ntegra Aura microscope working in atmospheric conditions (air temperature 21°C, pressure 1000 hPa). NT-MDT NSG10/Au cantilevers coated with 35 nm layer of Au. The setup was connected electrically with the sample to provide the positive bias on the cantilever. Such setup allowed both for imaging the topography of the samples in the non-contact mode and EFM measurements. Each of the images were collected with 256 x 256 pts resolution. Results were analyzed using Gwyddion 2.40 software²².

C. Raman Spectroscopy and Optical Microscopy

Sample illumination, Raman measurements and Optical Microscopy were performed using Renishaw inVia system equipped with Olympus MPLN100x objective with 100x magnification and automated XYZ translation stage with 100 nm spatial resolution. Renishaw RL532C50 single mode laser with a nominal 45 mW output power has been used as an excitation source. Coupled with the optical microscope it allows to create a focused spot with the measured power of 13 mW and diameter of about 500 nm on the surface of the sample. This setup allowed for acquisition of optical images as well as high-resolution Raman measurements and provided the illumination source to the chosen areas of the sample. The obtained Raman spectra were analyzed by numerical fitting of the model spectrum basing on Lorentzian curves using Wolfram Mathematica 11.2 software.

III. RESULTS AND DISCUSSION

A. Electric field measurements

The results presented in this section were obtained on the h-BN/SiO₂ sample. This part of the experiment was performed in order to confirm that the modification is related to the emergence of the local electric fields in the sample. For this purpose a h-BN fragment with large area flat surface was selected. Its optical microscopy image is shown in Figure 1 a). Basing on the optical contrast the thickness of the sample is about 5 μm on the terraces with several higher topographical features¹⁸. The thickness and surface characteristics are further confirmed by AFM topography measurements seen in Figure 1 c).

The sample has been illuminated in a linear series of points, as indicated in Figure 1 b), with conditions that,

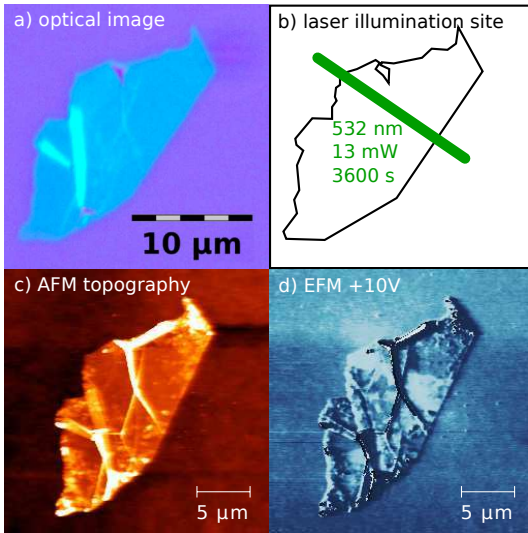


FIG. 1. a) Optical image of the h-BN flake on h-BN/SiO₂ sample, b) Schematic view of the flake with path of the laser illumination indicated with a green line, c) AFM topography of the h-BN flake, d) EFM image of the sample after illumination acquired with 10 V positive bias between AFM cantilever and sample.

as we believed, would maximize the observed modification of the local characteristics of the h-BN fragment. Each of the points was separated from each other by 500 nm distance. They were illuminated with 532 nm laser with 13 mW power on the spot with about 500 nm radius (power density of about $16.5 \text{ mW}\mu\text{m}^{-2}$) over the time span of 3600 seconds.

The topography presented in Figure 1 c) has been acquired after the illumination process. It shows some topographical features that were not seen in during the optical measurements - few wrinkles of the h-BN material and slight amount of residues left after the deposition process. However, no distinct features can be found where the illumination was conducted. This clearly shows that despite using the high-power density radiation the sample has not been damaged and shows no visible signs of degradation or deposition of the contamination on the surface. The correlation between the sample illumination and the electric field emergence, however, can be clearly seen during EFM measurements, as presented in Figure 1 d). In the image the bright area can be seen where the sample was illuminated indicating the presence of electric interaction between the surface and the cantilever. This clearly proves that the incidence of the focused laser light onto hexagonal boron nitride causes changes in the charge carrier distribution within this material and leads to emergence of local electric fields. As shown later in this article this effect may be used to control the characteristics other 2D materials present in the vicinity of the modified h-BN by means of the field-effect with non-invasive method of illumination with high-power density light.

B. Time-resolved Raman measurements

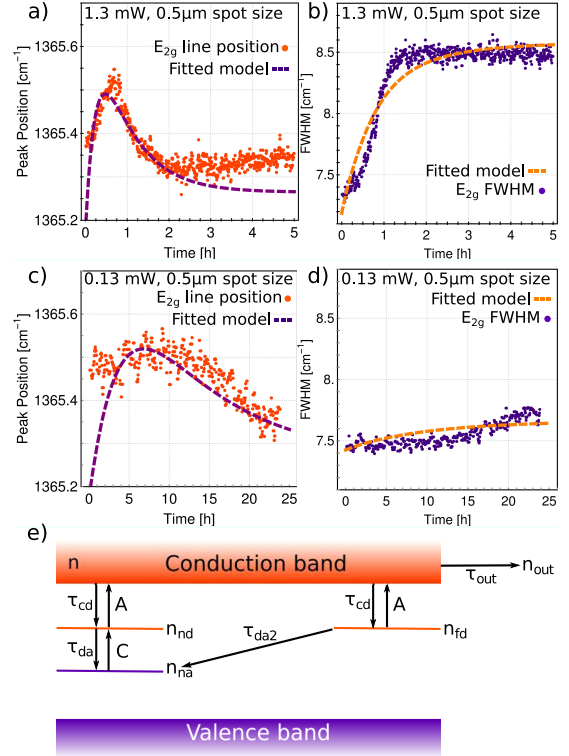


FIG. 2. Changes of a, c) position and b, d) FWHM of E_{2g} Raman line of h-BN during the illumination with 532 nm laser with of a, b) 1.3 mW power and $0.5 \mu\text{m}$ spot size and c, d) 0.13 mW power and $0.5 \mu\text{m}$ spot size respectively. Purple, dashed line and orange, dashed line presented in a) and b) are the theoretical model fitted to the results. e) the schematics of the electron transitions between the defect centers in illuminated h-BN assumed in the theoretical model describing the observed photo-ionization of the h-BN.

Results presented in the previous chapter proved that the laser illumination of the hexagonal boron nitride leads to the emergence of the local electric fields. However, in order to fully utilize this phenomenon to control other Van Der Waals materials within the heterostructure it is important to identify the processes behind this phenomenon as well as investigate the dynamics of the occurring changes. For this purpose in-situ Raman Spectroscopy measurements have been performed on the h-BN/SiO₂ sample. The exfoliated flake has been modified in several points with a focused beam of 532 nm laser. The optical filters have been used in order to adjust the power densities to the desired levels. The illuminating beam has been used to induce the Raman scattering effect for whole duration of the modification process. The time of acquisition for each of the spectra has been adjusted to reach satisfactory signal-to-noise ratio. Each of the spectra has been fitted with a Lorentzian curve, which has been used to describe the spectral line related

to the E_{2g} vibrational mode of h-BN, which is located at the Raman shift of about 1365 cm^{-1} ²³. The model results of this experiment are presented in Figure 2 a) and b).

The changes of the position of the E_{2g} line are seen in Figure 2 a). The initial position of 1365.4 cm^{-1} is related to the several factors, such as the thickness or its initial charge state of the h-BN fragment¹⁸. During the first hour of the illumination the E_{2g} line is shifted towards the higher values, eventually reaching the peak value of about 1365.55 cm^{-1} . After that point the line is shifted downwards to about 1365.3 cm^{-1} after 2 hours of the process. Subsequently, the line is shifted toward higher values again, albeit at much slower rate.

The changes can also be seen in the FWHM of the E_{2g} line (as seen in Figure 2 b). This parameter starts at about 7.5 cm^{-1} and quickly increases to about 8.5 cm^{-1} after nearly 2 hours into the process. Next, the width of the spectral line seems to be reaching stable level and does not undergo any changes within the time of observation.

The described behavior can be explained by the modifications of the charge state of deep defects induced by the illumination. In the proposed model we assume the donors to be of a shallow type and delocalized within the area of several lattice constants and, therefore, with limited coupling to the lattice. On the other hand, strongly localized deep acceptor centers can substantially influence h-BN structure upon the charge transfer induced by photo-ionization. Thus, we associate the observed shifting of the Raman line energy with the concentration of acceptors in neutral state^{24 ? ,25}.

In the simplified model we assume the presence of defect levels²⁶ related to acceptors with concentration N_A and donors with concentration $N_D + N_A$. We assume that our sample is n-type and in thermodynamic equilibrium concentration of ionized donors and acceptors are the same and equal to N_A . It was shown²⁷ that Coulomb coupling and an additional short-range interaction promote the tendency toward self-compensation by the formation of donor-acceptor pairs. Due to the Coulomb interaction the minimum energy of the system is reached when ionized are the donors nearest to the ionized acceptors. Therefore we divide the donor centers into two groups: "near" - located near acceptor states, initially ionized, with concentration N_A and "far" - initially neutral, located far from the acceptors, with concentration of N_D . The incidence of light onto the crystal may change this equilibrium state. In the simplest model, with the excitation below the energy gap, we take into account the excitation that transforms the ionized donor-acceptor pair into neutral one with probability rate C (Figure 2 e) and excitations of neutral donors which create free electrons in conduction band with the probability rate A , the same for both near and far donors (Figure 2 e). As a recombination processes we take into account donor acceptor recombination for near donors with the recombination τ_{da} , as well as between far neutral donor and neutral acceptor with significantly bigger recombination time τ_{da2} . Free

electrons from the conduction band, within our model can either be trapped by ionized donor with the recombination time τ_{cd} or escape outside the illuminated part, with the escape time τ_{out} . We apply a limit N_Z to the concentration of electrons that can escape from the illuminated region. To describe this effect we solve the set of rate equations for the described system

$$\frac{dn_{nd}(t)}{dt} = Cn_{na}(t)(N_A - n_{nd}(t)) - \frac{1}{\tau_{da}}n_{nd}(t)(N_A - n_{na}(t)) - An_{nd}(t) + \frac{1}{\tau_{cd}}n(t)(N_A - n_{nd}(t)) \quad (1)$$

$$\frac{dn_{fd}(t)}{dt} = -\frac{1}{\tau_{da2}}n_{fd}(t)(N_A - n_{na}(t)) - An_{fd}(t) + \frac{1}{\tau_{cd}}n(t)(N_D - n_{fd}(t)) \quad (2)$$

$$\frac{dn_{na}(t)}{dt} = \frac{1}{\tau_{da2}}n_{fd}(t)(N_A - n_{na}(t)) - Cn_{na}(t)(N_A - n_{nd}(t)) + \frac{1}{\tau_{da}}n_{nd}(t)(N_A - n_{na}(t)) \quad (3)$$

$$\frac{dn(t)}{dt} = An_{nd}(t) - \frac{1}{\tau_{cd}}n(t)(N_A - n_{da}(t)) + An_{fd} - \frac{1}{\tau_{cd}}n(t)(N_D - n_{fd}(t)) - \frac{1}{\tau_{out}}n(t)(N_Z - n_{out}(t)) \quad (4)$$

$$\frac{dn_{out}(t)}{dt} = \frac{1}{\tau_{out}}n(t)(N_Z - n_{out}(t)) \quad (5)$$

where: n_{nd} and n_{fd} are the concentration of electrons present on near and far donors respectively, n is the free electron concentration in the conduction band, n_{na} is the concentration of negatively ionized acceptors, that are treated as the source of electrons that can be excited to the near donor. n_{out} is the concentration of electrons that escape from illuminated part of the sample.

TABLE I. The initial parameters of the model.

Parameter	Initial value
$n_{nd}(0)$	0
$n_{fd}(0)$	N_D
$n_{na}(0)$	N_A
$n(0)$	0
$n_{out}(0)$	0

We assume that each excitation and recombination process is proportional to the concentration of the occupied initial states and to the concentration of empty final states. Only to the concentration of the empty states in

the conduction band we do not apply any limits. Considering equations 1-5 it is possible to calculate the changes in the occupation in each of the considered states. We solved numerically this set of equations with the initial parameters presented in Tab. I.

We assume that the position of the E_{2g} line ($E(t)$) is tied strictly to the strain of the h-BN lattice. The redistribution of the charge carriers leads to emergence of the non-uniformity of the electric fields within a crystal, which distort the lattice by means of piezoelectricity²⁸. We assume that the changes of the position of the E_{2g} line are related to the number of neutral acceptor centers ($N_A - n_{na}(t)$), therefore the position of the line can be expressed with equation 6

$$E(t) = a(N_A - n_{na}(t)) + E_0 \quad (6)$$

where E_0 is the position of the E_{2g} line in the initial state and a is the scaling parameter. It is worth noting that similar correlation between the illumination and the changes in crystalline structure is found in other semiconductors, such as GaN [?], $GaAs$ ^{24?} or $AlGaAs$ ²⁵.

The full width of half maximum of the E_{2g} line is related to the local disorder in the lattice of the illuminated h-BN. We assume the disorder is introduced primarily by the presence of the ionized defect centers ($N_D - n_{nd}(t) + (N_D - n_{fd}(t)) + n_{na}(t)$), which create non-uniform electric fields in the crystal leading to rise of the disorder. This effect is lowered by the fact that the electron-dipole interaction depends on the distance between those two objects, therefore the dipole contribution can be written as $R \frac{n_{nd}(t)(N_A - n_{na}(t))}{N_A}$, where R is the parameter relative to strength of the dipole contribution into the effect. Therefore the FWHM ($\Sigma(t)$) of the E_{2g} Raman line is given by equation 7

$$\Sigma(t) = c(n_{nd}(t) + n_{fd}(t) + (N_A - n_{na}(t)) - R \frac{n_{nd}(t)(N_A - n_{na}(t))}{N_A}) + \Sigma_0 \quad (7)$$

where c is the scaling parameter and Σ_0 is the initial FWHM of the line.

The equations 6 and 7 have been fitted simultaneously to the data presented in figure 2 a) and b), with the result presented in the same images. Based on this the parameters have been estimated to those presented in Tab. II

Our simple model describes the experimental data reasonably well, in exception to the beginning of the process. This may indicate that the initial state of the system has been different than assumed. What is more, the number of possible levels associated with the defects in hexagonal boron nitride may be higher than what is taken into account in the model²⁶. Both of those effects may explain the mentioned discrepancy, particularly if the probabilities of electrons moving to and from them is high.

TABLE II. The fitting parameters for the model fitted to the changes of Raman line position and FWHM for illumination with 1.3 mW and 0.13 mW 532 nm laser.

Parameter	1.3 mW, 0.5 μm spot	1.3 mW, 0.5 μm spot
A	0.23 h ⁻¹	0.016 h ⁻¹
C	0.86 ⁻¹	0.06 h ⁻¹
τ_{cd}	1.5 h	10.5 h
τ_{da}	0.62 h	8.7 h
τ_{da2}	4.0 h	84 h
τ_{out}	2 h	28 h
N_A	1.5	1.5 a.u.
N_D	8.5	8.5 a.u.
N_Z	0.5	2 a.u.

Fitting to the data obtained during the illumination with 532 nm laser with power of 0.13 mW and spot size of 0.5 μm over a time span of 24 hours, as presented in figure 2 c) and d) results in the following values:

Again, the divergence from the data can be seen for the early stages of the observed process. What is more, it seems counterintuitive for the lifetimes, τ_{da} and τ_{da2} in particular, to change with the power density of the illuminating light. This fact can be explained by the possibility that all of the electron transitions may be mediated by the conductivity, valence bands or both. In this case the illumination may influence the mobility of the charge carriers which are transported in the sample. What is more, the changes in the illumination may result in shifting of the quasi Fermi level. While this model is simplified and does not take all of the factors into account, such as additional defect center levels, it does explain the major trends in the observed parameters within the investigated scope of the power densities and, therefore, in our opinion, gives an insight on the basic processes behind the changes observed in the experimental results.

While the threshold of the process is not seen in our results, there are more parameters that may have an influence on the process. One of those key aspects is establishing whether interaction between the h-BN layers are influencing the process. This is important both to the analysis of the physical process itself and the applications, where the thickness control issues is vital.

In order to investigate that aspect we conducted in situ Raman measurements on the exfoliated h-BN flake with areas of different thickness on sample h-BN/SiO₂ (see Figure 3 a) and a monolayer CVD h-BN fragment on G/h-BN/SiO₂ sample. The changes of the position of the E_{2g} Raman line are presented in Figure 3 b). It is worth noting that the initial state of the exfoliated flake investigated here, in particular the thicker area, was different from that presented in Figure 2, however the changes that can be seen are similar to those previously reported - after 1 hour of illumination the peak position decreases rapidly, and starts increasing slowly after reaching minimum value. The modification of the CVD (0.3 nm thickness) h-BN also seems to be progress-

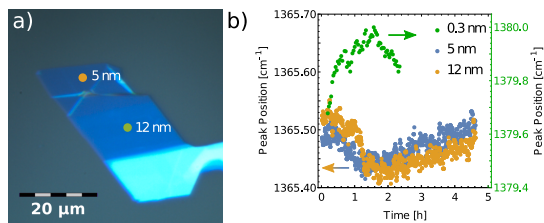


FIG. 3. a) Optical microscopy image of the investigated h-BN flake on h-BN/SiO₂ sample with points points of Raman measurements indicated with green and yellow dot, b) the dynamics of E_{2g} line position changes during the illumination on h-BN of different thicknesses - 0.3 nm (CVD monolayer h-BN, sample G/h-BN/SiO₂), 5 nm and 12 nm (sample h-BN/SiO₂).

ing with similar dynamics, however, the last phase is not seen, due to the long acquisition times needed to reach that phase - the local maximum appears after almost 2 hours of the illumination indicating that the photo-excitation occurs at slower rate in case of this sample. This effect is most likely related to the significant difference in thickness coupled with low absorption coefficient or the interaction of the boron nitride layers with the substrate.

C. Modification stability

The effect of photo-excitation of the charge carriers by the electromagnetic radiation within the hexagonal boron nitride has been previously investigated within the scope of the short-term effects, where the changes induced by light have been shown not to be stable and disappear after stopping the illumination²⁹. The effect described in this article, however, shows signs of the stability - the electric contrast measurements (seen in Figure 1 d) have been conducted few hours after the illumination, proving that the changes in the charge carrier distribution remain stable at least for that duration. However, in order to establish whether the created modifications will still be seen on the sample after longer times we conducted measurements on the h-BN/SiO₂ sample 5 months after the illumination.

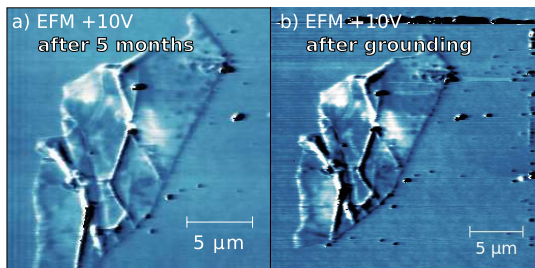


FIG. 4. EFM images of the illuminated h-BN flake on h-BN/SiO₂ sample after a) 5 months of time, b) electrical grounding of the sample.

The EFM image of the sample after that time is shown in Figure 4 a). It is clearly seen that the contrast has not changed and slight differences between the images in Figure 4 a) and Figure 2 d) can be attributed to the differences in the exact state of the used AFM tip and environmental conditions. This shows that the energy levels attributed to the defect centers²⁶, the charge state of which is influenced by the illuminations are deep and may be used to effectively trap the charge for extremely long times. This also proves that the field effect generated by the investigated effect may be used to permanently influence the heterostructure and may indicate the prospective applications of this effect where the stability of the effect is vital, such as the non-volatile memories or in nanostructured devices.

Additionally, the attempts at restoring the initial state of the illuminated h-BN have been performed. This has been done by performing the AFM scans of the surface with the tip with Au coating in the contact mode of AFM. The tip has been grounded electrically. After such attempts, however, the EFM contrast can still be seen (see Figure 4 b). This suggests that the procedure did not have a significant impact on the charge state of the material.

D. Response of graphene to h-BN modification

The last part of the analysis of the phenomenon of light-induced charge carrier photo-excitation in hexagonal boron nitride is investigation of the influence of the electric fields generated by the effect on graphene within the heterostructures composed of these two materials. The analysis of that effect is basing on the Raman Spectroscopy measurements. The spectra were gathered during the illumination conducted on both the heterostructures and the graphene layers on h-BN/G/SiC and G/h-BN/SiO₂ samples. Lorentzian curves were fitted to the G and 2D bands of the Raman spectra of graphene. Analysis of the parameters of the curves provides information on the charge carrier concentration and the mechanical strain on the material³⁰⁻³². In case of low n-type doping (under $2 \cdot 10^{13} \text{ cm}^{-2}$). Within those bounds energy of the G band depends on the electron concentration linearly and 2D is independent from this value. The energies of G and 2D band are related to mechanical strain (ϵ) and electron concentration (n) by equations 8 and 9³⁰, where γ_G and γ_{2D} are Grüneisen parameters for G and 2D bands respectively. $a = 7.38 \cdot 10^{13} \text{ cm}$ is a parameter calculated by linear fitting of $E_G(n)$ function for electrostatic gating and E_G^0 and E_{2D}^0 are the band positions of the undoped graphene for Raman measurements with 532 nm excitation wavelength. We assumed the γ_G/γ_{2D} to be equal to 0.71³⁰.

$$E_{2D} = E_{2D}^0 - 2\gamma_{2D} \cdot E_{2D}^0 \cdot \epsilon \quad (8)$$

$$E_G = E_G^0 - 2\gamma_G \cdot E_G^0 \cdot \epsilon + n \cdot a \quad (9)$$

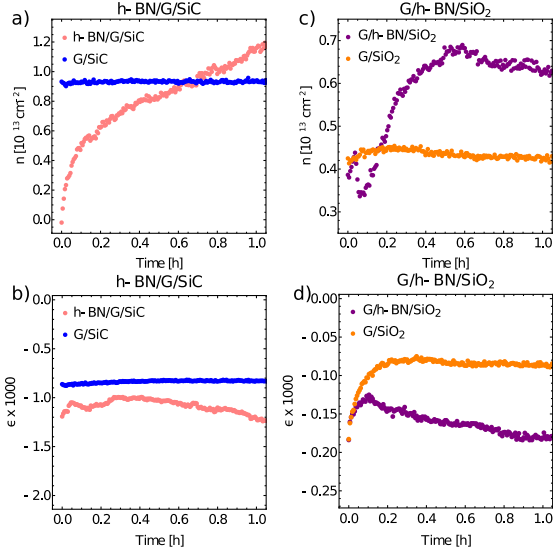


FIG. 5. Changes in the a, c) electron concentration and b, d) strain in graphene and graphene/h-BN heterostructure in a, b) h-BN/G/SiC and c, d) G/h-BN/SiO₂ samples.

The results of the measurements are shown in Figure 5. The differences in the reaction of the graphene and the heterostructures can be clearly seen at the first glance. During the entirety of the illumination the strain of the graphene outside the heterostructures, both in case of the epitaxial material on the native substrate (h-BN/G/SiC) and after the transfer (G/h-BN/SiO₂) show nearly no reaction, as shown in Figure 5 b) and d). The only observed small changes occur in the first 0.2 hours in case of the transferred material. This is most likely associated with the reaction of the non-relaxed interface to the changes in the charge state of hexagonal boron nitride. This also has an impact on the mobility of the graphene fragment on the surface. Increase of this parameter may allow the interface between graphene and surface to relax, which is consistent with the results seen in Figure 5 d). The change is very slight, however, reaching only 0.01 %. The reaction of the heterostructures is higher, which is related to the fact that, due to the presence of elevated temperatures, the interface between graphene and hexagonal boron nitride is changing leading to the alignment of the materials, which may also have impact on the electronic structure of the system^{33,34}. It is worth noting that in the case of relaxed graphene/h-BN interface the atomic distances are different from the free-standing material due to lattice mismatch and possibility of rotation in the alignment of the interface^{33,34}.

The major differences appear, however, in the electron doping of the investigated samples (see Figure 5 a) and c)). As was the case for the strain, the graphene outside of the heterostructures shows nearly no reaction to

the laser illumination in both of the investigated samples. The exact value of the doping is related to the fact that the material has been grown on different substrates leading to the different initial value of charge carrier concentration. In case of h-BN/G/SiC sample the concentration in graphene was at the level of about $0.9 \cdot 10^{13} \text{ cm}^{-2}$ (Figure 5 a)), while within the heterostructure this value was changing from 0 to $1.2 \cdot 10^{13} \text{ cm}^{-2}$ with decreasing rate. It is worth pointing out that the initial doping of the heterostructure is significantly different from freestanding graphene most likely due to the possibility of transfer of static charges to the system during exfoliation and transfer of the h-BN layers.

The evolution of the charge carrier concentration in G/h-BN/SiO₂ progresses similarly, however, there are few key differences, as shown in Figure 5 c). First, the change in the electron doping of the heterostructure is much smaller and is contained within the range of $0.35 \cdot 10^{13} \text{ cm}^{-2}$ to $0.70 \cdot 10^{13} \text{ cm}^{-2}$. This fact is understandable considering that the h-BN layer is much thinner and therefore there the density of the defect centers is lower. The generated field, which is associated with them is weaker and thus has lesser impact on graphene. The second difference lies in the fact that the electron concentration is decreasing after 0.6 hours. As before that time the character of the changes is similar to that in Figure 5 a). It is likely that the rate of changes is different. Again, this can be attributed to the fact that in the G/h-BN/SiO₂ sample we are dealing with the monolayer material, which is related to the lower maximum charge carrier concentration in the defect levels.

Basing on the above results it can be clearly seen that the presence of the h-BN causes the modification of the charge carrier concentration in graphene during the illumination with high power density light. As the reaction of the freestanding graphene is significantly lower the changes can be attributed to the emergence of the non-uniform electric fields in h-BN. The above results show that the electron concentration can be changed in wide range (from 0 to 10^{13} cm^{-2}) therefore it shows that it is possible to control the electric conductivity of the heterostructure using the illumination with high power density light opening the possibilities of application of the effect in data storage or electronic element and circuit engineering. What is more, as the photo-excitation effect occurs in h-BN it may also be used it in tailoring the properties of other 2D materials.

IV. CONCLUSIONS

In summary it has been shown that the illumination of the hexagonal boron nitride leads to the emergence of the local electric fields. This effect has been attributed to the transitions of the electric charge carriers within this material between the levels associated with the structural defects. Those defect levels have been proven to be located deep within the band gap of the h-BN. Because

of this fact the light-induced modification of the charge carrier concentration has been shown to be stable within long periods of time.

The results presented in this article show that the electric fields appearing in h-BN may be used to control the properties in other 2D materials, which can be used to construct the heterostructures with hexagonal boron nitride. In particular, the presented results show the influence of illumination on graphene/h-BN heterostructure, where the electric field may be used to control the electron concentration in graphene.

The described effect allows for easy and non-invasive tailoring of the electronic properties of the two-dimensional materials and may open new directions of research of the Van Der Waals heterostructures and their applications.

V. ACKNOWLEDGMENTS

This work was supported by National Science Centre project granted on the basis of the decision number DEC-2015/16/S/ST3/00451. The work was also financially supported by National Science Centre project 2015/19/B/ST3/03142 as well as the European Union Seventh Framework Program (Grant. No. 604391 Graphene Flagship).

VI. REFERENCES

- ¹Hamed Nematian, Mahdi Moradinasab, Mahdi Pourfath, Morteza Fathipour, and Hans Kosina. Optical properties of arm-chair graphene nanoribbons embedded in hexagonal boron nitride lattices. *Journal of Applied Physics*, 111(9):093512, 2012.
- ²Simon Lu and Alan J. H. McGaughey. Thermal conductance of graphene/hexagonal boron nitride heterostructures. *Journal of Applied Physics*, 121(11):115103, 2017.
- ³Chao-Hui Yeh, Zheng-Yong Liang, Yung-Chang Lin, Tien-Lin Wu, Ta Fan, Yu-Cheng Chu, Chun-Hao Ma, Yu-Chen Liu, Ying-Hao Chu, Kazutomo Suenaga, and Po-Wen Chiu. Scalable van der waals heterojunctions for high-performance photodetectors. *ACS Applied Materials & Interfaces*, 9(41):36181–36188, 2017. PMID: 28945069.
- ⁴I Wlasny, M Rogala, P Dabrowski, P J Kowalczyk, A Busiakiewicz, W Kozlowski, L Lipinska, J Jagiello, M Aksienionek, Z Sieradzki, I Krucinska, M Puchalski, E Skrzetuska, Z Draczynski, and Z Klusek. Finding optimal HBr reduction of inkjet printed graphene oxide for flexible electronics. *MATERIALS CHEMISTRY AND PHYSICS*, 181:409–414, 2016.
- ⁵Kirsten T Winther and Kristian S Thygesen. Band structure engineering in van der waals heterostructures via dielectric screening: the gw method. *2D Materials*, 4(2):025059, 2017.
- ⁶M. Rogala, P. Dabrowski, P.J. Kowalczyk, I. Wlasny, W. Kozlowski, A. Busiakiewicz, I. Karaduman, L. Lipinska, J.M. Baranowski, and Z. Klusek. The observer effect in graphene oxide - How the standard measurements affect the chemical and electronic structure. *Carbon*, 103, 2016.
- ⁷A K Geim and K S Novoselov. The rise of graphene. *Nature materials*, 6(3):183–91, mar 2007.
- ⁸A. H. Castro Neto, N. M. R. Peres, K. S. Novoselov, and A. K. Geim. The electronic properties of graphene. *Reviews of Modern Physics*, 81(1):109–162, jan 2009.
- ⁹Jonas D. Buron, Filippo Pizzocchero, Peter U. Jepsen, Dirch H. Petersen, Jos M. Caridad, Bjarke S. Jessen, Timothy J. Booth, and Peter Bggild. Graphene mobility mapping. *Scientific Reports*, 5:12305–, July 2015.
- ¹⁰Young Jun Shin, Ryan Stromberg, Rick Nay, Han Huang, Andrew T.S. Wee, Hyunsoo Yang, and Charanjit S. Bhatia. Frictional characteristics of exfoliated and epitaxial graphene. *Carbon*, 49(12):4070 – 4073, 2011.
- ¹¹G. Giovannetti, P. A. Khomyakov, G. Brocks, V. M. Karpan, J. Van Den Brink, and P. J. Kelly. Doping graphene with metal contacts. *Physical Review Letters*, 101, 2008.
- ¹²F Schwierz. Graphene transistors. *Nature Nanotechnology*, 5(7):487–496, 2010.
- ¹³M. L. Hu, J. L. Yin, C. X. Zhang, Zhizhou Yu, and L. Z. Sun. Electronic structures and optical properties of hexagonal boron nitride under hydrostatic pressures. *Journal of Applied Physics*, 109(7):073708, 2011.
- ¹⁴Hyun Jeong, Seungho Bang, Hye Min Oh, Hyeon Jun Jeong, Sung Jin An, Gang Hee Han, Hyun Kim, Ki Kang Kim, Jin Cheol Park, Young Hee Lee, Gilles Lerondel, and Mun Seok Jeong. Semiconductor-Insulator-Semiconductor Diode Consisting of Monolayer MoS₂, h-BN, and GaN Heterostructure. *ACS Nano*, 9(10):10032–10038, 2015.
- ¹⁵Ki Kang Kim, Allen Hsu, Xiaoting Jia, Soo Min Kim, Yumeng Shi, Mario Hofmann, Daniel Nezhich, Joaquin F. Rodriguez-Nieva, Mildred Dresselhaus, Tomas Palacios, and Jing Kong. Synthesis of monolayer hexagonal boron nitride on Cu foil using chemical vapor deposition. *Nano Letters*, 12(1):161–166, 2012.
- ¹⁶Matthew Yankowitz, Jiamin Xue, Daniel Cormode, Javier D. Sanchez-Yamagishi, K. Watanabe, T. Taniguchi, Pablo Jarillo-Herrero, Philippe Jacquod, and Brian J. LeRoy. Emergence of superlattice Dirac points in graphene on hexagonal boron nitride, 2012.
- ¹⁷K S Novoselov, A K Geim, S V Morozov, D Jiang, Y Zhang, S V Dubonos, I V Grigorieva, and A A Firsov. Electric field effect in atomically thin carbon films. *Science (New York, N.Y.)*, 306:666–669, 2004.
- ¹⁸Roman V. Gorbachev, Ibtisam Riaz, Rahul R. Nair, Rashid Jalil, Liam Britnell, Branson D. Belle, Ernie W. Hill, Kostya S. Novoselov, Kenji Watanabe, Takashi Taniguchi, Andre K. Geim, and Peter Blake. Hunting for monolayer boron nitride: Optical and raman signatures. *Small*, 7(4):465–468, 2011.
- ¹⁹T Uwanoo, Y Hattori, T Taniguchi, K Watanabe, and K Nagashio. Fully dry PMMA transfer of graphene on <i>h</i>-BN using a heating/cooling system. *2D Materials*, 2(4):041002, nov 2015.
- ²⁰W. Strupinski, K. Grodecki, A. Wyszomolek, R. Stepniewski, T. Szkopek, P. E. Gaskell, A. Grüneis, D. Haberer, R. Bozek, J. Krupka, and J. M. Baranowski. Graphene epitaxy by chemical vapor deposition on SiC. *Nano Letters*, 11:1786–1791, 2011.
- ²¹Ji Won Suk, Alexander Kitt, Carl W. Magnuson, Yufeng Hao, Samir Ahmed, Jinho An, Anna K. Swan, Bennett B. Goldberg, and Rodney S. Ruoff. Transfer of cvd-grown monolayer graphene onto arbitrary substrates. *ACS Nano*, 5(9):6916–6924, September 2011.
- ²²Nečas David and Klapetek Petr. Gwyddion: an open-source software for SPM data analysis , 2012.
- ²³S. Reich, a. Ferrari, R. Arenal, a. Loiseau, I. Bello, and J. Robertson. Resonant Raman scattering in cubic and hexagonal boron nitride. *Physical Review B*, 71(20):1–12, 2005.
- ²⁴P Trautman and J M Baranowski. Evidence for trigonal symmetry of the metastable state of the \textit{EL} 2 defect in GaAs. *Phys. Rev. Lett.*, 69(4):664–667, 1992.
- ²⁵M Leszczynski, T Suski, and G Kowalski. Dx centre and large lattice relaxation effects in algaas:te studied by x-ray diffraction. *Semiconductor Science and Technology*, 6(1):59, 1991.
- ²⁶Bing Huang and Hoonkyung Lee. Defect and impurity properties of hexagonal boron nitride: A first-principles calculation. *Physical Review B*, 86(24):245406, 2012.

- ²⁷P. Boguslawski and J. Bernholc. Doping properties of c, si, and ge impurities in gan and aln. *Phys. Rev. B*, 56:9496–9505, Oct 1997.
- ²⁸Mohammad Noor-A-Alam, Hye Jung Kim, and Young-Han Shin. Dipolar polarization and piezoelectricity of a hexagonal boron nitride sheet decorated with hydrogen and fluorine. *Physical chemistry chemical physics : PCCP*, 16(14):6575–82, 2014.
- ²⁹L Ju, J Velasco, E Huang, S Kahn, C Nosiiglia, Hsin-Zon Tsai, W Yang, T Taniguchi, K Watanabe, Y Zhang, G Zhang, M Crommie, A Zettl, and F Wang. Photoinduced doping in heterostructures of graphene and boron nitride. *Nature nanotechnology*, 9(5):348–52, 2014.
- ³⁰J. M. Urban, P. Dbrowski, J. Binder, M. Kopciuszyski, A. Wyszmoek, Z. Klusek, M. Jaochowski, W. Strupiski, and J. M. Baranowski. Nitrogen doping of chemical vapor deposition grown graphene on 4h-sic (0001). *Journal of Applied Physics*, 115(23):233504, 2014.
- ³¹Ji Eun Lee, Gwanghyun Ahn, Jihye Shim, Young Sik Lee, and Sunmin Ryu. Optical separation of mechanical strain from charge doping in graphene. *Nature Communications*, 3:1024–, August 2012.
- ³²Diedrich A. Schmidt, Taisuke Ohta, and Thomas E. Beechem. Strain and charge carrier coupling in epitaxial graphene. *Phys. Rev. B*, 84:235422, Dec 2011.
- ³³C. R. Woods, L. Britnell, A. Eckmann, R. S. Ma, J. C. Lu, H. M. Guo, X. Lin, G. L. Yu, Y. Cao, R. V. Gorbachev, A. V. Kretinin, J. Park, L. A. Ponomarenko, M. I. Katsnelson, Yu. N. Gornostyrev, K. Watanabe, T. Taniguchi, C. Casiraghi, H-J. Gao, A. K. Geim, and K. S. Novoselov. Commensurate-incommensurate transition in graphene on hexagonal boron nitride. *Nature Physics*, 10(6):451–456, 2014.
- ³⁴John R. Wallbank, Marcin Mucha-Kruczyński, Xi Chen, and Vladimir I. Fal'Ko. Moiré superlattice effects in graphene/boron-nitride van der Waals heterostructures, 2015.